Physically defined silicon triple quantum dots charged with few electrons in metal-oxide-semiconductor structures

Hiraoka, S.; Horibe, K.; Ishihara, R.; Oda, S.; Kodera, T.

DOI
10.1063/5.0010906

Publication date
2020

Document Version
Final published version

Published in
Applied Physics Letters

Applied Physics Letters

Physically defined silicon triple quantum dots charged with few electrons in metal-oxide-semiconductor structures

Cite as: Appl. Phys. Lett. **117**, 074001 (2020); https://doi.org/10.1063/5.0010906
Submitted: 15 April 2020 . Accepted: 10 August 2020 . Published Online: 19 August 2020

S. Hiraoka, K. Horibe, R. Ishihara, S. Oda, and T. Kodera

Applied Physics Letters ARTICLE scitation.org/journal/apl

Physically defined silicon triple quantum dots charged with few electrons in metal-oxide-semiconductor structures

Cite as: Appl. Phys. Lett. **117**, 074001 (2020); doi: 10.1063/5.0010906
Submitted: 15 April 2020 · Accepted: 10 August 2020 ·
Published Online: 19 August 2020

S. Hiraoka,[1] K. Horibe,[1] R. Ishihara,[2,3] S. Oda,[1] and T. Kodera[1,3,a)]

AFFILIATIONS

[1]Department of Electrical and Electronic Engineering, Tokyo Institute of Technology, Meguro, Tokyo 152-8552, Japan
[2]QuTech, Kavli Institute of Nanoscience and Faculty of Electrical Engineering, Mathematics and Computer Science, Delft University of Technology, Delft 2628CD, The Netherlands
[3]Quantum Computing Unit and Tokyo Tech World Research Hub Initiative, Institute of Innovative Research, Tokyo Institute of Technology, Meguro, Tokyo 152-8552, Japan

[a)]**Author to whom correspondence should be addressed:** kodera.t.ac@m.titech.ac.jp

ABSTRACT

Physically defined silicon triple quantum dots (TQDs) are fabricated on a silicon-on-insulator substrate by dry-etching. The fabrication method enables us to realize a simple structure that does not require gates to create quantum dot confinement potentials and is highly advantageous for integration. We observe the few-electron regime and resonant tunneling points in the TQDs by applying voltages to two plunger gates at a temperature of 4.2 K. Moreover, we reproduce the measured charge stability diagram by simulation with an equivalent-circuit model composed of capacitors and resistors. The equivalent-circuit simulation makes it clear that we realize three QDs in series within the nanowire, as planned. This circuit model also elucidates the mechanism of resonant tunneling and identifies a quadruple point of TQDs.

Quantum dots (QDs)[1,2] and double quantum dots[3–6] (DQDs) have been thoroughly studied aiming to understand quantum mechanical systems using electron spin states or charge states.[7] This effort was recently applied to a solid-state-based quantum bit (qubit), demonstrating full control of a single spin-qubit in DQDs with an additional structure that generates the necessary magnetic field for electron spin resonance (ESR).[8–11] Extending double QDs to triple QDs (TQDs) is essential for controlling and understanding multi-spin properties. The TQDs have their own unique physics. For example, a spin–spin interaction known as the Ruderman–Kittel–Kasuya–Yoshida interaction was observed in the TQDs.[12] It is also believed that they can be used to demonstrate quantum teleportation in spatially separated spin-entangled electron currents.[13] Furthermore, TQDs could be used as an implementation for qubits[14] because they provide a simple structure and scheme for single-qubit manipulation, which removes the necessity for the additional structure for ESR.[15,16] Such qubits are called exchange-only-qubits, and their simple structure is thought to be promising for integration in the future. From a material perspective, silicon TQDs are ideal for qubits in addition to understanding multi-spin physics. Electron spins in silicon have a long coherence time that is attributed to its being rich isotopes with zero nuclear spin.[17–31] Furthermore, silicon is compatible with classical CMOS processing. Thus, several studies have been conducted to date on silicon TQDs,[32–34] and universal coherent control of a qubit in silicon TQDs has actually been demonstrated.[32]

Silicon QDs, which were previously reported, were defined electrically in heterostructures or metal-oxide-semiconductor (MOS) structures with multi-layered fine gates. However, this fabrication method may have integration limitations because electrically defined TQDs need plunger gates as well as the gates defining the QDs, and a lot of lines (from 10 to 15) are required in order to work as a single qubit. These complicated gate patterns may prevent utilization of the essential advantage of exchange-only-qubits, that is, their simply integrable structure.

In this Letter, we report on an original fabrication technique to a TQD configuration.[35–37] This fabrication method enables us to realize a simple structure. We obtained small QDs in TQDs tunnel-coupled to reservoirs by improved techniques of electron-beam lithography, dry-etching, and thermal oxidation. As a result, we demonstrated the

operation of few-electron TQDs at a relatively high temperature of 4.2 K. Both few-electron states and higher temperature operation are important to integrate spin-based qubits in QDs. Furthermore, we have analyzed the behavior of the TQDs with a universal equivalent circuit agreement between the model and the experimental results of serial TQDs. The model makes it clear that we obtained three tunnel-coupled QDs in series as planned. We have also examined the transport mechanisms of resonant tunneling and co-tunneling through TQDs.

Scanning electron micrographs (SEMs) of the TQD device are shown in Figs. 1(a)–1(c). TQDs are located in the nanowires and have four intentionally constricted parts. A single electron transistor is used as a charge sensor (CS), and two plunger side gates (SGR and SGL) control the electrochemical potential in the TQDs. These plunger gates can be used for full single qubit control and they do not need any other gates such as those for forming the QD, which are necessary for the electrically defined QD. Thus, these TQDs are highly advantageous for integration. Figure 1(d) shows the schematic device structure. We fabricated a metal-oxide-semiconductor (MOS) structure composed of a gate insulator and a global top gate. We formed the gate insulator with a combination of thermal oxidation (10 nm) and low-pressure chemical vapor deposition (~50 nm). Thermal oxidation is performed at 1000 °C for 5 min to passivate the surface states of the silicon-on-insulator (SOI) layer and reduce the size of the QDs. Thus, the TQD device dimensions shown in the SEM image of Fig. 1(c) are slightly larger than the actual sizes of QDs in silicon. In order to show that the dimensions of the TQDs are shrunken by thermal oxidation, we oxidized the same patterns as in Fig. 1(c) with the same conditions and removed the SiO_2 passivation layer in hydrofluoric acid. The patterns before and after thermal oxidation and removing the passivation layer are shown in Figs. 1(a) and 1(b), respectively. The actual diameter of the QD after thermal oxidation is ~20 nm, which is much smaller than that of the TQDs reported in Ref. 33. The small size of both the QDs and the constricted parts is one of the important requirements for obtaining the few-electron regime in QDs. This is because the distance between the QDs is short, which can result in large inter-dot tunnel coupling. The QD-reservoir coupling strength is also important for finding the empty configuration. In our previous work reported in Ref. 33, the tunnel barriers were too opaque to obtain the few-electron regime. In this work, we improved the design of the side gates and the reservoirs as shown in Fig. 1(c). Because of the short distance between the QD and the gate, the side gate voltage V_{SGL} controls the potential of the left QD more efficiently and has less effect on the QD-reservoir coupling. Also, the reservoirs have been changed wider. This strengthened the QD-reservoir coupling. Even if a large negative voltage is applied to the side gate to expel electrons in the QD, the QD-reservoir coupling can be kept high enough.

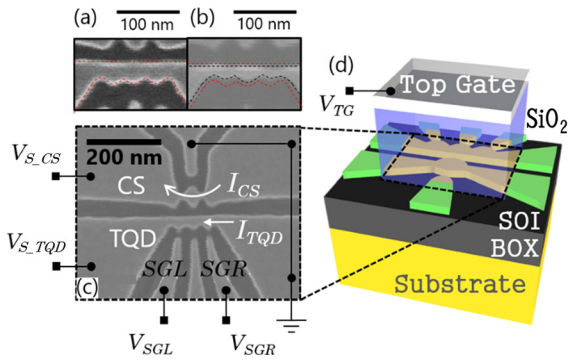

FIG. 1. (a) Scanning electron microscope (SEM) image of physically defined TQDs before thermal oxidation for passivation of the silicon on insulator (SOI) surface. The dark (bright) region consists of SiO_2 (Si). (b) SEM image of physically defined TQDs after the removal of the SiO_2 passivation layer. The red dashed lines indicate the shape of the TQDs in (a). It is clear that the TQDs become smaller by thermal oxidation for passivation. [(c) and (d)] Schematic measurement setups with the SEM image (c) and the schematic image (d) of the device. The transport current through the TQD is indicated by I_{TQD} and the charge sensor current is indicated by I_{CS}.

All measurements are performed at a temperature of 4.2 K with voltages fixed at $V_{TG} = 2.0$ V, $V_{S\_TQD} = 0.8$ mV, and $V_{S\_CS} = 3$ mV. Figures 2(a)–2(c) show the charge stability diagram of the TQDs as indicated by the CS signal dI_{CS}/dV_{SGL} as a function of V_{SGR} and V_{SGL}. The charge state of the TQD is indicated by parentheses (n, m, l), where n, m, and l are the number of electrons confined in the left, middle, and right dots, respectively. Blue and red stripes in Fig. 2(a) indicate Coulomb oscillation of the CS. In the oscillation, feature lines with three different slopes appear as expected. The slopes are determined by the coupling strength between each side gate and each QD within the TQDs. Therefore, the nearly horizontal yellow (nearly vertical purple) charging lines in Fig. 2(a) indicate charging events of the right (left) QD in Fig. 1(c), and the red charging line in Fig. 2(a) corresponding to the charging events of the middle QD has a slope of $dV_{SGR}/dV_{SGL} = -1$. Furthermore, we observe the few-electron regime in this stability diagram. The lack of charging lines in the lower left corner of the diagram indicates that the TQD is completely uncharged. Thus, this diagram enables us to determine an accurate number of electrons confined in each of the QDs within the TQD as a function of V_{SGR} and V_{SGL}. The charging lines indicated by the black arrows in Fig. 2(a) seem to have a different slope from all the main charging lines. These lines originally come from the charging lines of the middle QD (black dashed lines). In this region, there are no electrons in both the right and left QDs, and the tunneling barrier becomes very high. This makes the charging process of the middle QD slow, followed by

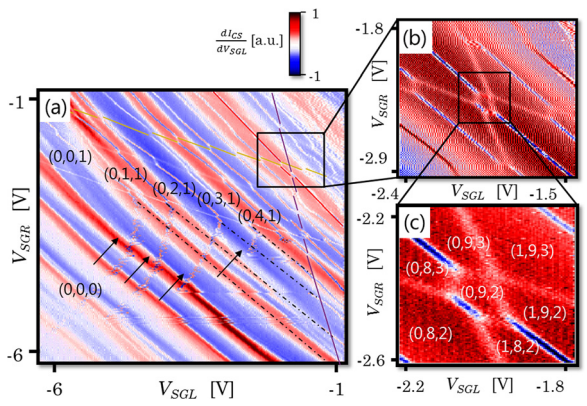

FIG. 2. [(a)–(c)] Transconductance dI_{CS}/dV_{SGL} of a CS as a function of V_{SGR} and V_{SGL}. Several charge transition lines appear in the background, which is Coulomb oscillation of the CS. The charge transition lines in (b) and (c) correspond to those of I_{TQD} plots shown in Figs. 3(a) and 3(b).

breaking of the charging lines. The slope of the broken lines depends on the sweep direction of V_{SGL} during the measurements.[38] All the crossings of the two charging lines are avoided due to the electrostatic inter-dot coupling. The spacing is determined by the inter-dot coupling energy E_m. We represent E_m between the left-middle QD, middle-right QD, and left-right QD as E_{mLM}, E_{mMR}, and E_{mLR}, respectively. The space of anti-crossings between (0,8,3)–(0,9,2) [(0,9,2)–(1,8,2)] in Fig. 2(c) indicates the inter-dot coupling between the left-middle QD (middle-right QD). Thus, E_{mLM} and E_{mMR} are nearly equal, and E_{mLR} can be ignored because the inter-dot coupling between left-right QDs indicated by the anti-crossing between (0,9,3)–(1,9,2) is negligible. These results are consistent with the geometric features of serial TQDs.

We measure I_{TQD} in Fig. 3(a) [Fig. 3(b)] simultaneously with a charge stability diagram in Fig. 2(b) [Fig. 2(c)]. Several charging lines in Fig. 3(a) [Fig. 3(b)] are traced from the charge stability diagram of Fig. 2(b) [Fig. 2(c)]. We observe three types of resonant tunneling points [such as points A, B, and C in Fig. 3(b)] in the I_{TQD} plots. In principle, the resonant tunneling transport of carriers in the TQDs is observed only at the charge quadruple point, where four charge configurations are degenerate; however, the transport can also be observed at the triple points in the TQDs when a higher-order tunneling process

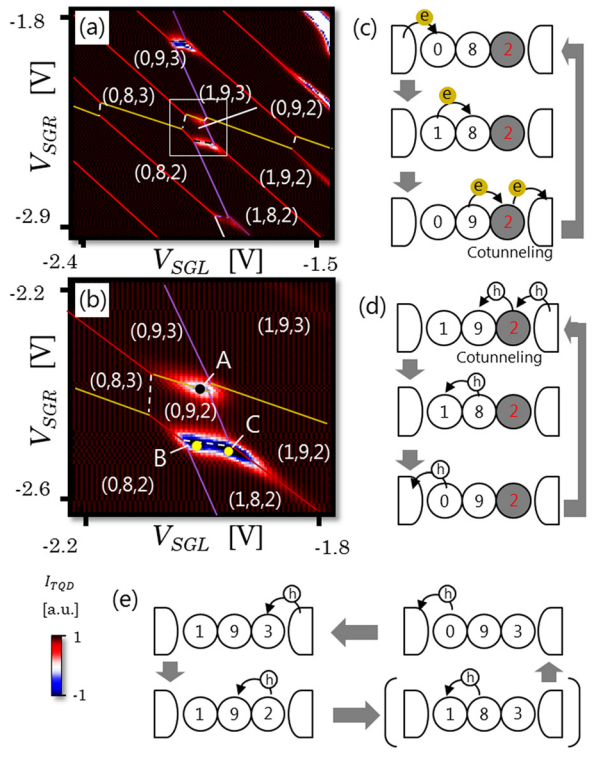

FIG. 3. (a) I_{TQD} plot as a function of V_{SGR} and V_{SGL}. The measurement is performed simultaneously with the charge stability diagram shown in Fig. 2(b). (b) Magnified plot of (a), measured simultaneously with Fig. 2(c). (c) Schematic diagrams of electron transportation processes at the triple point of B in (b). (d) Schematic diagrams of hole transportation processes at the triple point of C in (b). (e) Schematic diagram of the hole transportation process at the quadruple point of A in (b).

is permitted. Actually, the resonant tunneling points of B and C are the pair of "electron" and "hole" charge triple points attributed to the co-tunneling process.[3] The diagram in Fig. 3(c) represents resonant tunneling transport at point B. At this point, the electrons are transported and the (0,8,2), (1,8,2), and (0,9,2) charge configurations are degenerate due to the allowance of electron co-tunneling at the transition (0,9,2)–(0,8,2) in the right QD. At point C, hole current flows with (1,9,2), (1,8,2), and (0,9,2) degenerate charge configurations and co-tunneling occurs at the transition of (1,9,2)–(1,8,2) in the right QD, as described in Fig. 3(d). Along the purple charging line representing charging events of the left QD in Fig. 3(a), a pair of resonant transport points appear when the charging lines cross the red charging lines. The resonant transport mechanism of these pairs is the same as that of pair B and C and is caused by the co-tunneling process in the right QD. The remaining resonant tunneling transport at point A is a quadruple point, where (1,9,3)–(1,9,2)–(1,8,3)–(0,9,3) charging configurations are degenerate, as shown in Fig. 3(e). Note that the charge configuration of (1,8,3) is absent in the charge stability diagram. In the TQDs, charge configurations are determined by the electrochemical potentials of three QDs and a three-dimensional charge stability diagram is necessary in order to obtain full charge configurations. Thus, the absence of the specific charge configuration in the two-dimensional charge stability diagram naturally occurs.

We have analyzed the behavior by applying a Monte Carlo technique to the universal equivalent circuit model of serial TQDs with CS. The equivalent circuit model is composed of a capacitance and resistance network [Fig. 4(a)] in which the tunneling junction T_{Label} consists of the resistance R_{Label} and the capacitance C_{Label} in parallel, and the inter-dot coupling between middle and left (right) QDs is represented by the tunneling junction T_{12} (T_{23}). Our model is designed to simulate the total environment including the action of the CS. In other words, we can simulate the charge stability diagram of the TQDs by monitoring the CS current in the circuit model, i.e., the model performs a simulation under conditions that are closer to reality. Figure 4(b) [Fig. 4(c)] shows the calculated charge stability diagram with the same condition as that of Fig. 2(a) [Fig. 2(b)]. The calculated results show an excellent agreement with our measurements. This circuit model is designed to represent a serial TQD, where there are inter-dot couplings only between the middle and left (right) QDs, not between the right and left QDs. Its agreement with the measured results clearly shows that the left, middle, and right QDs are actually located in series within the nanowire fabricated.

In our circuit model, the resonant co-tunneling process is simulated by tunneling junctions (T_{2S} and T_{2D}) between the middle QD and the two reservoirs. In the resonant co-tunneling process at points B and C, where co-tunneling occurs in the right QD, current flows when the electrochemical potentials in the left and middle QDs are matched and act as if carriers are transported from the middle QD directly to the right reservoir. Thus, we describe this current path [PATH1 in Fig. 4(a)] by connecting the middle QD and the right reservoir using the tunneling junction T_{2S} and we use the circuit model to simulate the co-tunneling process of the right QD. In the simulation, we can arbitrarily switch the co-tunneling allowance by tuning the value of R_{2S} in the tunneling junction T_{2S}. Fig. 4(d) [Fig. 4(e)] shows the calculated I_{TQD} while co-tunneling events are permitted (inhibited). Here, we observe that the resonant points indicated by the white arrows are suppressed when the co-tunneling is inhibited.

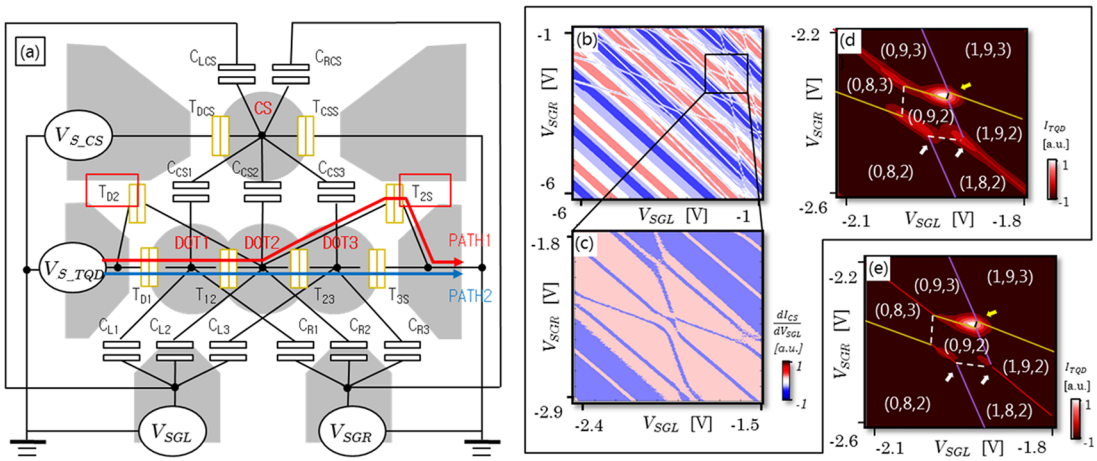

FIG. 4. (a) Equivalent circuit diagram for three tunnel-coupled QDs. The nodes DOT1, DOT2, and DOT3 refer to the left, center, and right dots, respectively. Tunnel barriers are modeled as resistors and capacitors in parallel. [(b) and (c)] Calculated transconductance dI_{CS}/dV_{SGL} of a CS from the equivalent circuit model. (d) Calculated I_{TQD} with co-tunneling events permitted. (e) Calculated I_{TQD} with co-tunneling events inhibited.

This result clearly shows that these resonant points are the triple points attributed to the co-tunneling process. On the other hand, in the resonant point indicated by the yellow arrow, the current flows independently of the allowance of co-tunneling. At this point, we can see that the carriers are transported through PATH2 in Fig. 4(a) and we can identify it as truly a quadruple point. From this simulation result, we conclude that the resonant point of A in Fig. 3(b) is a hole quadruple point where the (1,9,3)–(1,9,2)–(1,8,3)–(0,9,3) charging configurations are degenerate. Note that co-tunneling is either elastic or inelastic, simultaneous tunneling of two or more electrons, although in our model it is simulated with the non-quantal equivalent-circuit by just adding the tunneling junction T_{2S}. In our model, we are not able to discriminate between either elastic or inelastic contributions; however, it is a simple method to reproduce the transport properties in TQDs including resonant tunneling and co-tunneling.

Toward the exchange-only qubits, the tunability of the tunnel couplings is important. We can tune the tunnel coupling strength by controlling the size of the constricted parts in the fabrication, but *in situ* control is also necessary for operation of qubits. By applying the bias voltage between the source and drain contacts, the side gate voltages, and the top gate voltage, the tunnel coupling can be controlled. In order to obtain more tunability, it is desirable to attach the metal fine gates with high dielectric constant gate oxide on the constricted parts.

In conclusion, we have demonstrated the few-electron-regime in silicon TQDs at a temperature of 4.2 K. Key to this achievement is the fabrication technique, which enables us to form highly scaled-down QDs. Furthermore, modeling the TQDs with a capacitance network that includes the CS action, we have shown good agreement between the simulation and the experimental results. We have also examined the resonant tunneling transport of the TQDs and found the quadruple point. This study is the first step toward the realization of the exchange-only qubits using a physically defined silicon TQD, which is highly advantageous for integration.

This work was financially supported by JST-CREST (No. JPMJCR 1675), JSPS-KAKENHI Grants-in-Aid (No. 20H00237), and Quantum Leap Flagship Program (Q-LEAP) Grant No. JPMXS 0118069228 of the Ministry of Education, Culture, Sports, Science and Technology (MEXT) of Japan.

DATA AVAILABILITY

The data that support the findings of this study are available from the corresponding author upon reasonable request.

REFERENCES

[1]S. Tarucha, D. G. Austing, T. Honda, R. J. van der Hage, and L. P. Kouwenhoven, Phys. Rev. Lett. **77**, 3613 (1996).
[2]J. M. Elzerman, R. Hanson, L. H. Willems Van Beveren, B. Witkamp, L. M. Vandersypen, and L. P. Kouwenhoven, Nature **430**, 431 (2004).
[3]W. G. van der Wiel, S. De Franceschi, J. M. Elzerman, T. Fujisawa, S. Tarucha, and L. P. Kouwenhoven, Rev. Mod. Phys. **75**, 1 (2002).
[4]A. C. Johnson, J. R. Petta, C. M. Marcus, M. P. Hanson, and A. C. Gossard, Phys. Rev. B **72**, 165308 (2005).
[5]C. Barthel, D. J. Reilly, C. M. Marcus, M. P. Hanson, and A. C. Gossard, Phys. Rev. Lett. **103**, 160503 (2009).
[6]T. Kodera, K. Ono, Y. Kitamura, Y. Tokura, Y. Arakawa, and S. Tarucha, Phys. Rev. Lett. **102**, 146802 (2009).
[7]R. Hanson, L. P. Kouwenhoven, J. R. Petta, S. Tarucha, and L. M. K. Vandersypen, Rev. Mod. Phys. **79**, 1217 (2007).
[8]J. R. Petta, A. C. Johnson, J. M. Taylor, E. A. Laird, A. Yacoby, M. D. Lukin, C. M. Marcus, M. P. Hanson, and A. C. Gossard, Science **309**, 2180 (2005).
[9]F. H. L. Koppens, C. Buizert, K. J. Tielrooij, I. T. Vink, K. C. Nowack, T. Meunier, L. P. Kouwenhoven, and L. M. K. Vandersypen, Nature **442**, 766 (2006).
[10]M. Pioro-Ladrière, T. Obata, Y. Tokura, Y.-S. Shin, T. Kubo, K. Yoshida, T. Taniyama, and S. Tarucha, Nat. Phys. **4**, 776 (2008).
[11]S. Nadj-Perge, S. M. Frolov, E. P. A. M. Bakkers, and L. P. Kouwenhoven, Nature **468**, 1084 (2010).
[12]B. N. J. Craig, J. M. Taylor, E. A. Lester, C. M. Marcus, M. P. Hanson, and A. C. Gossard, Science **321**, 817 (2008).
[13]D. S. Saraga and D. Loss, Phys. Rev. Let. **90**, 166803 (2003).
[14]D. P. DiVincenzo, D. Bacon, J. Kempe, G. Burkard, and K. B. Whaley, Nature **408**, 339 (2000).
[15]L. Gaudreau, G. Granger, A. Kam, G. C. Aers, S. A. Studenikin, P. Zawadzki, M. Pioro-Ladrière, Z. R. Wasilewski, and A. S. Sachrajda, Nat. Phys. **8**, 54 (2012).

[16]J. Medford, J. Beil, J. M. Taylor, S. D. Bartlett, A. C. Doherty, E. I. Rashba, D. P. DiVincenzo, H. Lu, A. C. Gossard, and C. M. Marcus, Nat. Nanotechnol. **8**, 654 (2013).
[17]G. Feher, Phys. Rev. **114**, 1219 (1959).
[18]C. Tahan, M. Friesen, and R. Joynt, Phys. Rev. B **66**, 035314 (2002).
[19]E. Abe, K. M. Itoh, J. Isoya, and S. Yamasaki, Phys. Rev. B **70**, 033204 (2004).
[20]A. M. Tyryshkin, S. A. Lyon, A. V. Astashkin, and A. M. Raitsimring, Phys. Rev. B **68**, 193207 (2003).
[21]A. M. Tyryshkin, S. Tojo, J. J. Morton, H. Riemann, N. V. Abrosimov, P. Becker, H. J. Pohl, T. Schenkel, M. L. Thewalt, K. M. Itoh, and S. A. Lyon, Nat. Mater. **11**, 143 (2012).
[22]J. J. Pla, K. Y. Tan, J. P. Dehollain, W. H. Lim, J. J. Morton, D. N. Jamieson, A. S. Dzurak, and A. Morello, Nature **489**, 541 (2012).
[23]B. M. Maune, M. G. Borselli, B. Huang, T. D. Ladd, P. W. Deelman, K. S. Holabird, A. A. Kiselev, I. Alvarado-Rodriguez, R. S. Ross, A. E. Schmitz, M. Sokolich, C. A. Watson, M. F. Gyure, and A. T. Hunter, Nature **481**, 344 (2012).
[24]E. Kawakami, P. Scarlino, D. R. Ward, F. R. Braakman, D. E. Savage, M. G. Lagally, M. Friesen, S. N. Coppersmith, M. A. Eriksson, and L. M. K. Vandersypen, Nat. Nanotechnol. **9**, 666 (2014).
[25]D. Kim, Z. Shi, C. B. Simmons, D. R. Ward, J. R. Prance, T. S. Koh, J. K. Gamble, D. E. Savage, M. G. Lagally, M. Friesen, S. N. Coppersmith, and M. A. Eriksson, Nature **511**, 70 (2014).
[26]X. Hao, R. Ruskov, M. Xiao, C. Tahan, and H. Jiang, Nat. Commun. **5**, 3860 (2014).
[27]M. Veldhorst, J. C. C. Hwang, C. H. Yang, A. W. Leenstra, B. de Ronde, J. P. Dehollain, J. T. Muhonen, F. E. Hudson, K. M. Itoh, A. Morello, and A. S. Dzurak, Nat. Nanotechnol. **9**, 981 (2014).
[28]M. Veldhorst, C. H. Yang, J. C. C. Hwang, W. Huang, J. P. Dehollain, J. T. Muhonen, S. Simmons, A. Laucht, F. E. Hudson, K. M. Itoh, A. Morello, and A. S. Dzurak, Nature **526**, 410 (2015).
[29]K. Takeda, J. Kamioka, T. Otsuka, J. Yoneda, T. Nakajima, M. R. Delbecq, S. Amaha, G. Allison, T. Kodera, S. Oda, and S. Tarucha, "A fault-tolerant addressable spin qubit in a natural silicon quantum dot," Sci. Adv. **2**(8), e1600694 (2016).
[30]J. Yoneda, K. Takeda, T. Otsuka, T. Nakajima, M. R. Delbecq, G. Allison, T. Honda, T. Kodera, S. Oda, Y. Hoshi, N. Usami, K. M. Itoh, and S. Tarucha, Nat. Nanotechnol. **13**, 102 (2018).
[31]J. Yoneda, K. Takeda, A. Noiri, T. Nakajima, S. Li, J. Kamioka, T. Kodera, and S. Tarucha, Nat. Commun. **11**, 1144 (2020).
[32]K. Eng, T. D. Ladd, A. Smith, M. G. Borselli, A. A. Kiselev, B. H. Fong, K. S. Holabird, T. M. Hazard, B. Huang, P. W. Deelman, I. Milosavljevic, A. E. Schmitz, R. S. Ross, M. F. Gyure, and A. T. Hunter, Sci. Adv. **1**(4), e1500214 (2015).
[33]R. Mizokuchi, S. Oda, and T. Kodera, "Physically defined triple quantum dot systems in silicon on insulator," Appl. Phys. Lett. **114**, 073104 (2019).
[34]M. Tadokoro, R. Mizokuchi, and T. Kodera, "Pauli spin blockade in a silicon triangular triple quantum dot," Jpn. J. Appl. Phys., Part 1 **59**, SGGI01 (2020).
[35]G. Yamahata, T. Kodera, H. Mizuta, K. Uchida, and S. Oda, Appl. Phys. Express **2**, 095002 (2009).
[36]K. Horibe, T. Kodera, and S. Oda, Appl. Phys. Lett. **106**, 053119 (2015).
[37]K. Horibe, T. Kodera, and S. Oda, Appl. Phys. Lett. **106**, 083111 (2015).
[38]C. H. Yang, N. S. Lai, R. Leon, W. H. Lim, and A. S. Dzurak, Appl. Phys. Lett. **105**, 183505 (2014).